ORIGINAL ARTICLE

DOI: https://doi.org/10.18599/grs.2021.3.14

Russian Original 2021. Vol. 23. Is. 3. Pp. 109–117

Passive seismic data processing methods to identify contrast intrasalt interlayers in the geological section of the Astrakhan Arch

E.V. Biryaltsev[1], *A.A. Vikhoreva*[2], *V.A. Zakharchuk*[3], *A.Yu. Komarov*[3], *V.V. Pykhalov*[2*], *O.V. Tinakin*[3]

[1]*Gradient Technology LLC, Kazan, Russian Federation*
[2]*Octopus LLC, Astrakhan, Russian Federation*
[3]*Gazprom dobycha Astrakhan LLC, Astrakhan, Russian Federation*

Abstract. The article examines the problem of processing microseismic noise (MN) to identify and evaluate occurrence depth of contrasting geological objects – intersalt interlayers with a potentially high formation pressure. If it is impossible to use artificial wave sources, statistic processing of passive seismic data becomes critical. Due to the accumulation of power spectral density (PSD) during a long-term recording of MN the deterministic medium effect on a random signal spectrum is identified. PSD modulation when the surface or the bottom of the layered medium is exposed to white noise is expressed in terms of the Green's function (GF) of a wave equation. Relevant GF variations corresponding to the layers form the basis for accumulated PSD approximation, and indicate the depth and contrast of the target features.

Keywords: hydrodynamically isolated layers, intersalt interlayers, formation pressure, passive seismic, low-frequency seismic sounding, microseismic noise, Green's function of a wave equation, power spectral density, collection of statistical information, maximum likelihood method

Recommended citation: Biryaltsev E. V., Vikhoreva A. A., Zakharchuk V. A., Komarov A. Yu., Pykhalov V. V., Tinakin O. V. (2021). Passive seismic data processing methods to identify contrast intrasalt interlayers in the geological section of the Astrakhan arch. *Georesursy = Georesources*. 23(3), pp. 109–117. DOI: https://doi.org/10.18599/grs.2021.3.14

Introduction

The territory of the Astrakhan Arch is the largest resource base of the Russian sector of the Peri-Caspian Depression (Antipov et al., 2008). The main explored hydrocarbon (HC) reserves within the Astrakhan arch are concentrated in the Bashkirian pay thickness. The total initial resources attributable to the subsurface deposits of the Astrakhan arch amount to 14.34 billion toe (tons of oil equivalent) (Novikov et al., 2007). The Astrakhan gas and condensate field (AGCF), a giant field located in the arch central part known as Aksaraisk swell, was discovered and is being developed. Apart from it, several large hydrocarbon deposits were discovered at the margins of the Aksaraisk swell: West Astrakhanskoye and Velikoye (Fig. 1). There are direct hydrocarbons indicators detected in some of these areas. There are direct hydrocarbons indicators detected in some of these areas.

The difficulties which challenge the development and exploration of the deposits are related to the penetration of complex deposits located over the productive zone. The thick mass over the productive zone, about 4000 m, has complex geology consisting of 12 stratigraphic horizons – from Quaternary to Lower Permian deposits, represented by terrigenous, carbonate, and sulfate-halogen rocks.

Most of the drilling problems are associated with advancing the Kungurian salt-bearing strata.

We can pick three formations in the structure of the Kungurian salt strata: the lower, sulfate-carbonate (the Filippovian horizon) formation; the middle, sulfate-carbonate-terrigenous (SCT), and the upper, halogen one. The middle and upper formations form the Iren horizon.

The sulfate-carbonate-terrigenous formation is represented by alternating members of gypsum, anhydrite containing a nonuniform inclusion of terrigenous-carbonate material, intrasalt clays, mudstones, limestones, and mixed-type rocks (sulfate-terrigenous and terrigenous-sulfate) dissected by interlayers of halite. The SCT formation is underlain by the lower subhorizontal mass of the Filippovsky horizon, represented by interlayers of limestones, clay limestones, anhydrites with interbeds of terrigenous material. The SCT formation is overlain by a halogen formation represented by rock salt and halite with occasional interlayers of non-halide rocks.

Often, the halogen formation is topped by the upper sulfate-carbonate caprock member, represented by sulfate-carbonate rocks.

*Corresponding author: Viktor V. Pykhalov
Email: viktor.pihalov@yandex.ru

The SCT formation features the presence of non-halide rocks members separated by salt intervals of various thicknesses. These members are hydrodynamically isolated beds (HIBs) which can contain high-pressure brine-saturated rocks.

According to well-logging and drilling data, HIB corresponds to intervals in the Lower Iren, represented by one or several layers of non-halogen rocks and separated from each other by impenetrable rocks of small thickness (15 meters or less). HIB can contain brine-saturated interlayers, where the formation pressure exceeds the downhole pressure (abnormally high-pressure layers). Penetration of these formations causes emergencies associated with brine showings. During the construction of production and exploration wells, drilling problems connected with brine showings from HIB were registered in more than 50 wells.

Responding to these emergencies requires significant material and technical costs and time. In some cases, wells must be abandoned.

Drilling with extra-heavy drilling muds from a depth of 2900 meters (minimum depth of the Lower-Iren SCT formation) can cause the hydro-frac effect in the layers with a lower pressure resulting in drilling problems, emergencies, and shut-down.

To avoid and minimize the risks of drilling problems, it is essential to have knowledge about HIBs, their number within the well section (estimated thickness of HIBs, penetration depths, and HIBs number). This data allows to develop in advance accident-preventive measures, update geomechanical modeling data.

Geological structure of the study target

Prediction of HIBs with 2D, 3D seismic, and CDP is quite challenging. In the seismic wavefield, the Kungurian sulfate-carbonate-terrigenous formation is imaged as chaotically distributed events, featuring increased energy as related to the wavefield which is common for suprasalt deposits (Fig. 2).

It is almost impossible to interpret such a complex wave pattern due to the following reasons:

- significant distortions of the seismic wave field caused by the complex structure of salt domes. Distortions are associated with the steep angles and dramatically changing curvature of salt walls (which are refracting and scattering boundaries), and with the small size of salt domes arches as compared to other survey apertures used in seismic. These factors lead to a significant non-hyperbolicity of reflected waves hodographs, and significant scattering effect of seismic energy;
- the influence of various noise events (scattered waves, diffracted waves, and others);
- irregularity of physical and morphological parameters of intrasalt members and intercalations.

The sections of the wells where brine showings were successfully eliminated were analyzed to identify the structural features of high-pressure HIBs. There were 37 such wells.

Well logging and drilling data analysis has shown that brine-saturated intervals (i.e., intervals with high-pressure brine-saturated formations) can be either independent HIBs or have several hydrodynamically isolated formations.

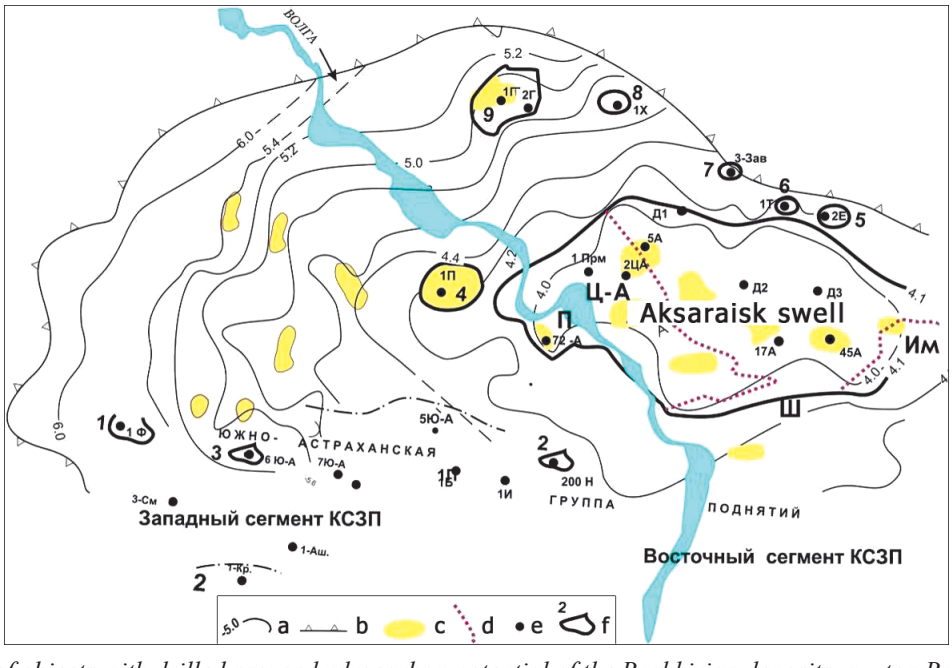

Fig. 1. The layout of objects with drilled proven hydrocarbon potential of the Bashkirian deposits. a – top Bashkirian isohypses; b – top Bashkirian carbonate mass outline; c – local fracturing zone ; d – boundaries of the AGCF segments: П – Pravoberezhny (right-bank); Ц-А – Centralno-Astrakhanskiy (Central Astrakhan); Л – Levoberezhny (left-bank); Ш – Shagalinsky; Им – Imashevsky; e – wells; f – structures (objects) with HC indications: 1 – Fersmanskaya; 2 – Nikolaevskaya; 3 – Ulanskaya; 4 – Pravoberezhnaya; 5 – Elenovskaya; 6 – Tabakovskaya; 7 – Zavolzhskaya; 8 – Kharabalinskaya; 9 – Selitrenno-Georgievskaya.

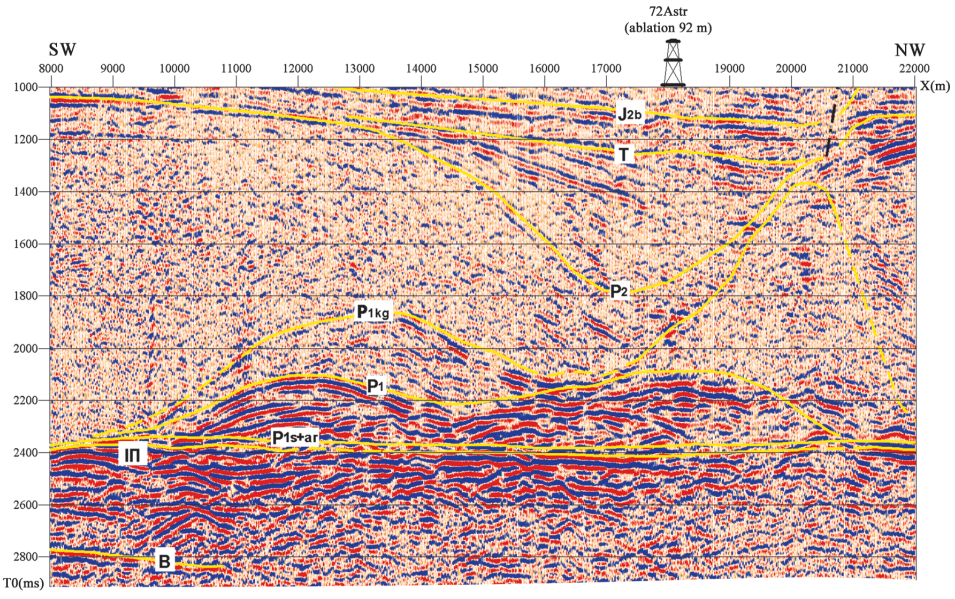

Fig. 2. Imaging of the lower formation (the mass between the horizon P1-P1a) in the seismic wave field. The right-bank segment of the Astrakhan arch.

The Kungurian halogen deposits are screens for HIBS in the brine-saturated intervals. These deposits overlay intercalations of non-halogen rocks (fractured anhydrites, rocks of mixed type (sulphate-carbonate and sulphate-terrigenous intercalations), intra-salt clays), acting as a reservoir of brine.

In some cases, anhydrites with no open fractures can be the screens for HIBs.

Based on the results of the geophysical surveys data analysis along with the data from the mud logging stations, 37 well sections showed 52 high-pressure brine saturated hydrodynamically isolated formations.

Statistical analysis of these data showed that more than 92 % of all identified HIBs are associated with anhydrite intercalations, 74 % are associated with the occurrence of intrasalt clays, and 70 % are characterized by mixed rocks occurrence. In general, more than 90 % of HIBs have two or more intercalations of rocks of various lithology.

Accordingly, HIBs represented by only one lithotype (anhydrite layer, mixed rocks layer, intrasalt clay layer) are relatively rare.

The boundaries of rocks with different lithotypes have different acoustic impedance and, and, consequently, have different reflection coefficient (Table 1).

According to well logging data, elastic waves velocity in the salt mass is 4500–4600 m/s. The salt density varies from 2.1 g/cm^3 to 2.2 g/cm^3 and can be assumed to be 2.15 g/cm^3 on average.

For sulfate-halogen and anhydrite rocks, the velocity of longitudinal waves varies from 5300 m/s to 5800 m/s, density – from 2.6 g/cm^3 to 2.8 g/cm^3. Sulfate-terrigenous and terrigenous-sulfate rocks are characterized by a change in the velocity of longitudinal waves from 4600 to 4800, 4800 m/s, density 2.4–2.55 g/cm^3. Intrasalt clays are characterized by the velocity of longitudinal waves, on average equal to 4200 m/s and a density of 2.4 g/cm^3.

The calculated positive reflection coefficients based on these averaged features (Table 2) showed that the intrasalt interlayers have significant reflection coefficients compared to the host rock (mostly halite). At the same time, the highest reflection coefficient will be found with HIBs associated with anhydrites – either in the top (salt/anhydrite boundary), or in the bottom (clay/anhydrite). The reflection coefficients for these boundaries are 0.23–0.25. The boundary clay/mixed rocks will feature a high reflection factor.

Clay/halite and mixed rocks/anhydrite boundaries are less defined.

As a rule, HIBs represented by several lithotypes have at least three layers with four acoustically contrasting interfaces (two with positive and two with negative reflection factors). HIBs represented by only one lithotype will have only two acoustically contrasting interfaces (with one positive and one negative reflection factor, respectively).

Kref	Layer top	Bottom
0.23	Halite	Anhydrite, halogenic-sulphate rocks
0.16	Halite	Mixed type rocks
0.25	Clay	Anhydrite, halogenic-sulphate rocks
0.072	Mixed type rocks	Anhydrite, halogenic-sulphate rocks
0.18	Clay	Mixed type rocks
0.019	Clay	Halite

Table 1. Calculated reflection coefficients for the boundaries associated with HIBs

No.	Well No.	HIB prediction based on LFS		HIB based on well logging TVDSS		Prediction mis-tie		Prediction estimation
						Top, m	Bottom, m	
1	**X1**	3500	3590	3507.9	3579.8	7.9	10.2	+
2	**X2***	3150	3225	3132.46	3182.76	17.54	42.24	+
3		3550	3650	3510.66	3554.06	39.34	95.94	+
4	**X3**	3175*	3200*	3156	3172.3	19	27.7	+
5		-	-	3264.9	3341.1	-	-	©
6		3450	3500	3504.6	3532.3	54.6	32.3	+
7		3500	3550	3532.3	3556.6	32.3	6.6	+
8		3625	3650	3580.3	3694.6	44.7	44.6	+
9		-	-	3694.6	3742.1	-	-	©
10	**X4**	3025	3050	3019.83	3028.03	5.17	21.97	+
11		3250	3325	3258.43	3324.93	8.43	0.07	+
12		3425	3450	3385.63	3419.23	39.37	30.77	+
13		3550	3625	3560.93	3645.63	10.93	20.63	+
14		3725	3750	3691.13	3744.83	33.87	5.17	+
15	**X5**	3200	3225	3124	3139.2	76	85.8	+
16		3375	3400	3331.5	3337.7	43.5	62.3	+
17		3400	3425	-	-	-	-	Δ
18		3425	3500	3538.2	3550.3	113.2	50.3	+
19		3550	3575	3550.3	3591.4	0.3	16.4	+
20		3725	3750	3737.3	3740.1	12.3	9.9	+
21		3750	3800	3740.1	3767	9.9	33	+
22	**X6**	2825	2850	2780.6	2822.6	44.4	27.4	+
23		-	-	2984.6	3036.6	-	-	©
24		3200	3225	-	-	-	-	Δ
25		3325	3350	3343	3387.8	18	37.8	+
26		3400	3450	3387.8	3418.6	12.2	31.4	+
27		-	-	3532.6	3616.4	-	-	©
28		-	-	3633	3677.9	-	-	©
29		3750	3775	3677.9	3707.4	72.1	67.6	+

*Table 2. Prediction vs Drilling data HIB prediction: + confirmed by well logs; Δ not confirmed by well logs; © not identified. *The forecast is only for assessing connectivity of these two layers with the high-pressure layers of the nearby well 915Ф.*

Another important feature is HIB thickness. Non-halogen intervals Another important feature is HIB thickness. Non-halogen intervals containing high-pressure layers have a thickness of 3 m to 240 m. Herewith, brine saturated intervals can be either independent HIBs or have several HIBs.

In the vast majority of cases, 63 % of HIBs have a thickness of 40 m and are represented by several lithotypes.

17 brine saturated intervals have a thickness of fewer than 40 meters, and 6 of them (35 %) have one lithotype.

Analysis of the anomaly ratio calculated based on the drilling mud density showed that its value is not related either to a HIB, or a brine saturated interval thickness. Any connection between the value of the brine saturated interval anomaly ratio and the salt bodies morphology has not been observed either. High-pressure brine saturated layers are identified both within the extension of salt bodies domes, and their flanks and downfolds.

The studies have shown a general trend – the increase in the thickness of the salt body is accompanied by the increase in the cumulative thickness of the sulfate-terrigenous carbonate formation increases (respectively, and the number of critically high-pressure layers).

The linear approximation factor is 0.4, that is, we can say about only a certain trend. While there are many cases where the thickness of the salt body is more than 3500 meters, and the non-halitic part is next to zero (i.e., sulfate-terrigenous carbonate formation is absent). Thus, the morphological criterion cannot be used for HIBs prediction.

Well logging analysis of the wells located at 1 km from each other shows that the number and thickness of non-halogen layers building up the sulfate-terrigenous carbonate formation, and their lithology are sharply variable laterally and vertically. This makes inter-well

correlation of such interlayers based on drilling and well logging data impossible in most cases.

In rare cases, it is possible to identify extended layers which are clearly identified between two wells. These data indicate that HIBs lateral dimensions do not exceed 2 kilometers, and in most cases, lateral dimensions do not exceed 1 kilometer.

The determination of the intra-salt bedding angle was done in a limited number of wells. Complete core analysis for the whole penetrated section was done in only three wells. In some wells the analysis was done only for selected coring intervals.

In some wells bedding angle can be determined with induction stratalfissured inclination survey method that identifies attitudes and fractures.

As a result of these surveys, it was found that the predominant occurrence of intra-salt layers is subhorizontal. At the same time, in several wells there were some intervals, underlain and overlain by halite, with intrasalt interlayers at angles of more than 30^0. It was noted that the wells intervals with subhorizontal occurrence can alternate with the intervals with intra-salt interlayers with the bedding angle of more than 300. Thus, the prediction of HIBs with potential high-pressure layers comes down to identifying acoustically contrasting interfaces corresponding in most cases to the top and bottom of HIBs, or single reflections (for the HIBs having one lithotype).

Due to the ineffectiveness of active seismic and interwell correlation methods, passive seismic survey technology was applied for the prediction of HIBs within the Kungurian salt-bearing sediments.

The proposed approach

Currently, theoretical methods of passive seismic, in particular, the method of low-frequency seismic sounding (LFS), analysis, and processing of field microseismic noise (MN) are described in the works (Birialtsev et al., 2009; Grafov et al., 1996). These works deliver direct modeling of the three-dimensional medium Green function and detailed statistical analysis of noise. These works also propose compensation of the surface wave signal at the vertical component of each receiver.

The assumption about the source at the deep surface and relation between transmissivity and approximation of primary event GF G(t), providing there are several minor reflectivity factors (Claerbout, 1968) lie at the core of the generalized LFS (low–frequency seismic sounding method) – interferometry (Draganov et al., 2003). Interferometry method principles are being developed in some works (Vidal et al., 2018) and cover a wide range of seismic exploration and monitoring objectives.

With all LFS methods, acquisition geometry shall include an areal arrangement (array) of 3C-receivers with a precise projection orientation XYZ, that is linked to spatial resolution (bearing) of wave propagation directions. Selection based on wave arrival direction is required for exclusion from processing both surface waves dominated by industrial noise, and head waves or body waves reflected at large angles, since they were not exposed to reflections from the target objects, and their acoustic paths lie mainly outside the section under study. The seismic array phasing allows rotation of the main beam of an antenna and obtaining weighted sums of signals (waves) of different directions. In this case, only waves with vertical range have informative value. The pattern synthesis and the separation of signals according to direction were carried out in the theory of digital antenna arrays (hereinafter – DAA) (Haykin, 1985).

An important element of LFS is the identification of vertically directed resonant waves in the natural acoustic field. These fields are formed at acoustically contrasting boundaries and resonate in the geological medium. The mass between the surface and the reflector is acting as a resonator.

Problem statement in primary event approximation

We are going to solve the problem of identifying contrasting objects in a rather known geological medium under the following conditions. Let us assume a horizontally homogeneous semi-infinite[1] model of the medium with the known visco-elastic characteristics, where N thin causative bodies (layers) with near-typical rheological characteristics and thickness are occurring at certain depths. This kind of research objective is typical for a survey of thin extended, but discontinued inclusions (deposits, intrusions) in a plane-parallel geological medium. These inclusions can be found at known depth ranges and are placed with the artifactually input uniform depth spacing.

Let $G(t;z,z')$ – the Green function (FG) section for a semi-infinite medium when the source and receiver are located on the surface: $z = z' = 0$, $G(t) = G(t;0,0)$. Under fixed spatial arguments, the GF is the impulse response in the time domain and the integrated response in the spectral representation.

For a homogeneous half-space, we have a basic GF $G_0(t)$, if there is an i-th layer:

$$G(t) = G_0(t) + \sum_{i=1}^{N} m_i \, \delta G_i(t) \quad (1)$$

where m_i is a function of the object presence taking on the value 1, if it is present in the medium, and on the value 0, if it is absent. Let us consider next the Fourier transform $\tilde{G}(\omega)$ for the $G(t)$

$$\tilde{G}(\omega) = \tilde{G}_0(\omega) + m_i \delta \tilde{G}_i(\omega) = \tilde{G}_0(\omega)\big(1 + m_i S_i(\omega)\big) \quad (2)$$

[1]The OZ axis of the Cartesian coordinates is directed vertically downwards, the coordinate z ϵ [0, +∞) corresponds to the depth.

where $\tilde{G}_0(\omega)$ and $\delta\tilde{G}_i(\omega)$ are complex Fourier images of the GF $G_0(t)$ and variations of the GF $\delta G_1(t)$ correspondingly, relative disturbance:

$$S_i(\omega) = \delta\tilde{G}_i(\omega)/\tilde{G}_0(\omega) \quad (3)$$

Hereinafter, summing over the indices *i, j,* repeated in the right-hand is conducted within the limits of 1 to *N*, where *N* is the number of layers.

2.2. The spectral density of the Green's function

We construct the spectral power density (PSD) of the medium frequency response, or the GF squared absolute value:

$$P(\omega) = \left|\tilde{G}(\omega)\right|^2 = \tilde{G}(\omega)\,\tilde{G}(-\omega)$$

Note that $\tilde{G}^*(\omega) = \tilde{G}(-\omega)$, using the formulas (2, 3), we will get:

$$P(\omega) = P_0\,\Big(1 + m_i S_i(\omega) + m_i S_i(-\omega) + m_i m_j S_i(\omega) S_j(-\omega)\Big) \quad (4)$$

where $P_0 = |G|^2$, considering that according to the problem setting $|\delta G_i| << |G_0|$, ($|S_1| << 1$), we can ignore the square term in (4):

$$P(\omega) = P_0\,\Big(1 + 2m_i\Re\big(S_i(\omega)\big)\Big)$$

$$P(\omega) + i\mathcal{H}[P](\omega) = P_0\,\big(1 + 2m_i S_i(\omega)\big) \quad (5)$$

where $\mathcal{H}[\cdot]$ is the Hilbert transformation. As we can see from the second formula (5) the analytical form of a real even function $P(\omega)$ is expressed in terms of complex relative variations (3) of the Green function (2). The definition of $\delta G_i(\omega)$, in general, does not lend itself to analytical calculation, but for flat layers it is possible to derive the transfer function of reflection from the layer.

2.3. Reflection from a single layer in a homogeneous medium

First, let us consider the case with a homogeneous medium (in half-space) with a single causative body. The frequency dependence $\delta\tilde{G}_i(\omega)$ can be constructed as a compound reflection coefficient from a layer with a thickness h_i at depth H_i. If *R* is the reflection coefficient from the layer top, then the reflection coefficient from the bottom is opposite in sign. Coefficients of transmission through the layer boundary: T^+_i – into the layer, T^-_i – outside the layer. Phasing constant with a wave double pass between the layer boundaries are expressed in terms of transit time $\tau_i = h_i/v_i$, $t_i = H_i/v_0$, where v_i, v_0 – phase velocities of waves. As a result, we get a model of the reflection frequency response[2]:

$$\delta\tilde{G}_i(\omega) = K_i(\omega)\,R_i\,\left(1 - T_i^+ T_i^- e^{-i2\omega\tau_i}\right)\,e^{-i2\omega t_i} \quad (6)$$

where $K_i(\omega)$ is the complex frequency response of the medium from the surface to the layer and from the layer to the surface, excluding the travel time. The coefficient of reflection from the top layer and the coefficients of the transmission into the layer and from the layer into the medium, respectively:

$$R_i = \frac{z_i - z_0}{z_i + z_0},\; T_i^{\pm} = 1 \pm R_i \quad (7)$$

where $z_i = p_i v_i$ is the impedance, *p* is the medium density.

Variations $\delta\tilde{G}_i(\omega)$ of are clearly identified only in the low-frequency range, below the lower limit of traditional seismic signals sources, which is usually 8÷10 Hz. With a natural source, the observations data represent natural microseismic noise (MN), its spectral density is a random function. The modulation of the spectrum caused by the object is a change in the random function, therefore, in order to detect the object, it is necessary to rearrange the data processing in such a way as to eliminate the response randomness effect. The use of MN in the LFS method provides for the accumulation of a large volume of information for the calculation of statistical characteristics, primarily, correlation functions.

Using the GF of a horizontal homogeneous medium, we record the response from an arbitrary source distributed on the surface *f(t):*

$$u(t) = \int dt'\,G(t - t')\,f(t') \quad (8)$$

Similarly, the response from the source at the lower boundary is recorded. Taking into account (8), we form the product of the values $u(t_1)$ and $u(t_2)$, then we average both parts of equality on the random-process realization of (SP) of the source, FG is deterministic and is taken out of the brackets of the averaging $\langle\cdot\rangle$:

$$\langle u(t_1)\,u(t_2)\rangle = \int dt_1' \int dt_2'\; G(t_1 - t_1')\,\langle f(t_1')\,f(t_2')\rangle\,G(t_2 - t_2') \quad (8)$$

Autocorrelation functions (ACF) approximation is the average products:

$$\mathcal{B}_k(\tau) = \langle u(t_1)\,u(t_2)\rangle_k,\; \mathcal{F}_k(\tau) = \langle f(t_1')\,f(t_2')\rangle_k \quad (10)$$

where bringing to the stationary form is provided by the introduction of difference time variables $\tau = t_1 - t_2$ and average time $s_k = \langle(t_1 + t_2)/2\rangle$, where s_k is the time point of the middle of the averaging window (frame), *k* is the frame number.

Thanks to the dependence $\mathcal{F}_k(\tau)$ from difference time $\tau = t_1 - t_2$, the convolution (9) is transformed to[3]:

$$\mathcal{B}_k(\tau) = G(\tau) * \mathcal{F}_k(\tau) * G(-\tau) \quad (11)$$

In the spectral domain (11) will be written as: $B_k(\omega) = \tilde{G}(\omega)F_k(\omega)\,\tilde{G}(-\omega)$. In the scalar case the latter equality can be written using the PSD:

[3]With a non-stationarity of the source, this convolutional formula is not accurate, but it can be used for the cases with the source ACF slow change over the average time variable, as compared to the difference time rate of change (i.e., compared to the change in the correlation interval).

[2]The variation of the Green function corresponding to the layer (object) can have a more complex form, amplitude and phase spectra of this variation fully characterize the layer reflecting properties. Depending on the type of the host geological formation, inclusions (deposits) can have non-trivial rheology, thanks to which the phase-frequency transformation between incident and reflected signals occurs.

$$B_k(\omega) = P(\omega)\, F_k(\omega),\ P(\omega) = \tilde{G}(\omega)\tilde{G}(-\omega) \quad (12)$$

Thanks to the linearity of (8), we can form any moment response function that is related to the source function of the same name via polynomial from the GF. The determinacy of the moment function with respect to RP leads to an equation for the GF, in the simplest case of the form (12), if there is an expectation (EXP) $\mathbf{E}[F_k(\omega)] = \mu(\omega)$. Consequently, the known moment function of the source RP acts as a deterministic source, which allows getting the GF from the MN measurements.

2.4. Solving the problem of layers presence as signal parameters estimation

Real microseismic noise is characterized by a significant and approximately identical spectral density in the ranges of 1 to 5÷10 Hz, which drops dramatically in the higher frequency range (Fig. 3).

Based on formulas (5) and (12), we can propose a method to identify survey targets with known characteristics in a generally known geological section.

When using expressions (5) and (12), we should take into account that for a single field measurement $B_k(\omega)$, the variance of the registered signal is intolerably large. For this reason, it is necessary to average over a set of observation frames, and that will reduce variance by n times, where n is the number of frames. Averaging procedure (12) over n-frames leads to the equation:

$$\bar{B}_n(\omega) = P(\omega)\, \bar{F}_n(\omega) \quad (13)$$

where accumulated average values are defined as standard arithmetic averages for the first n frames, during the measurement n increases:

$$\bar{B}_n(\omega) = \frac{1}{n}\sum_{k=1}^{n} B_k(\omega),\ \bar{F}_n(\omega) = \frac{1}{n}\sum_{k=1}^{n} F_k(\omega) \quad (14)$$

The PSD of a random process is the sum of the squares of two normally distributed RP with zero EXP and the same finite variance. It is known (Marple, 2003) that the process $\{F_k(\omega),\ k \in \mathbb{N}\}$ has exponential probability density function with parameter $\lambda=1/\mu$, MO $\mathbf{E}F(\omega) = \mu$, and the variance $\mathbf{D}F(\omega) = \mu^2$. According to the central limit theorem proved in probability theory, the variance of the accumulated average decreases by n times: $\mathbf{D}\bar{F}_n(\omega) = \mu^2/n$

The computational task involves the approximation of PSD, which is accumulated during measurements of microseismic noise using the representation (5) of the corresponding spectral density $P(\omega)$. Preliminary numerical modeling of the basic GF $G(\omega)$ and variations $\delta G_l(\omega)$ for positions significant from the geological point of view of leads (causative bodies) is required.

The coefficients m_i determined in the formula (1) can be interpreted as a degree of the object identification, including its thickness and contrast as compared to the lead with the reference thickness and contrast. When solving the inverse problem for intercalations identification, together with the reflection intensity (response amplitude), an estimate of the occurrence depth (or response delay time) for each layer is required. The number of intercalations which can be identified is unknown in advance. Therefore, the solution can be formulated as an estimation of the signal parameters, represented as a linear combination with the coefficients m_i of the basic transfer functions $S(\omega)$ of the thin layers located with the same depth interval. The m_i coefficients vector, providing the best stable approximation of the field PSD, shows the time and depth section as a result of processing passive seismic observations data.

To estimate the parameters of m_i, the maximum likelihood method was applied (Kramer 1975). The problem of PSD approximating is a mis-tie minimization: $|\bar{Z}_n(\omega) - m_i \boldsymbol{S}_i(\omega)|^2 \to min$, where $\bar{Z}_n(\omega)$ is oscillatory value as compared to analytical basic accumulated value of the field PSD:

$$\bar{Z}_n(\omega) = \frac{1}{2}\left(\frac{\bar{B}_n(\omega) + \boldsymbol{i}\mathcal{H}[\bar{B}_n](\omega)}{P_0(\omega)\,\mu(\omega)} - 1\right) \quad (15)$$

Thus, if the geological model of the host medium is known (including the geometry, interval characteristics (the speed of P-waves and S-waves, density), and an assumed location of the lead, then we can build vertical waves field models with different locations of the lead.

If we remove all waves, apart from vertical resonance ones, identified in the natural wave field, then, other factors being equal, the sum amplitude-frequency spectrum of the generated vertical waves both from a thin layer (e.g., as a HIB), and reflectors will differ from the same with the absence of a thin layer (e.g. a HIB).

Comparison of the model fields with the results of the observed vertical resonant waves field allows determining leads presence and location.

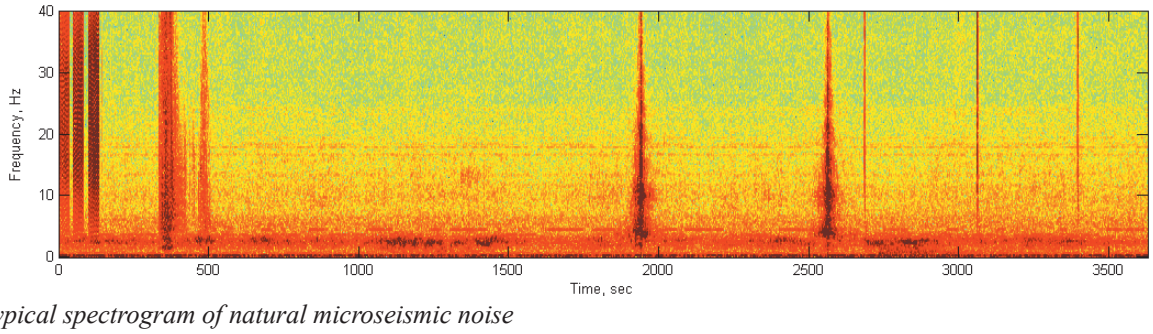

Fig. 3. Typical spectrogram of natural microseismic noise

Results

The proposed approach was applied to identify thin, acoustically contrasting brine saturated layers in the salt sequence at the pre-design stage of the deep drilling project at the AGCF.

Field works at the project wells sites was carried with LE-3D/5s seismometers, which record the natural wave field in the frequency from 0.2 Hz, the dynamic range is 140 dB. The works were carried out on a rectangular grid with 250 m spacing. Processing was carried out on a supercomputer running on graphic processors with the LINPACK performance of 36.6 Tflops.

In order to solve the problem concerning identifying and mapping the intersalt HIBs, a theoretical model of the geological medium with the HIB presence was constructed, based on well logging and VSP data, comprising structural and interval model of the principal acoustically contrasting interfaces, as well as an average statistical HIB model.

In accordance with the data given in section 1 of this article, the following model has been generated, showing the most potential HIB in the research area:

1. The HIB thickness is 75 meters;
2. The HIB is limited by layers at its top and bottom (25 meters thick each). The rocks composing the layers are characterized by a positive reflection coefficient with respect to the host medium;
3. The HIBs are overlapped and are underlain by the Kungurian galitic rocks. It should be noted that for such a model HIBs are synonymous with the definition of a brine-saturated interval.

The parameters of the host medium and its composing layers were determined for the modal HIB.

The selection of parameters was based on well logging data (see section 1 of the present article), and on the results of the survey works for HIBs identification in the area with the HIBs already identified (based on the results of the previously drilled wells).

As a result of matching the parameters for the host medium and for the layers composing the HIBs the following values were obtained:

- for the host medium, elastic waves velocity is 4600 m/s, the density is 2.15 g/cm^3;
- for the layers (HIBs indicators) located in the HIBs top and bottom, the P-waves velocity is 4800 m/s, the density is 2.6;
- for the layer enclosed between the layers in the HIB top and bottom the parameters assumed are the same as for the host medium;
- the thickness of the layer in the HIB top and bottom is 25 meters.

The field data were processed according to the standard processing graph using LFS method.

We calculated the model of the response from the host medium of the HIB model in the subsurface and with its presence at different depths.

The wave pattern obtained as a result of the field data processing was compared with the modeling results, and that allowed to determine the HIBs most probable locations and to predict their presence in the area of the project wells.

The forecasts were issued before the penetration of the Kungurain sediments. Figure 4 shows examples of the LFS and drilling results comparison.

As it can be seen from the figure, hydrodynamically isolated layers correspond to the identified increased LFS amplitudes. At the same time, the identified HIBs have a small thickness and local distribution, which is confirmed by the drilling data from a large number of wells.

The Table 2 shows the results of the retrospective estimation on the released prediction accuracy. The actual results show that the accuracy of the forecast is more than 75 %. The average error in HIBs top depth assessment is 40 m.

The results of HIBs prediction in complex conditions of salt-dome tectonics confirm LFS method efficiency for thin layers identification.

Conclusions

The practical works performed based on the developed technique for identifying a deterministic signal in the form of resonant vertical waves indicate the following:

The practical application of the LFS method to solve the problem of thin, high-pressure hydrodynamically isolated layers identification in the sequence of salt diapirs showed a high sensitivity of the method, in particular, it can identify acoustically contrasting members having a thickness of 25m and above.

Retrospective estimates of the HIB prediction showed (Table 2) that the HIB probability based on the LFS amounted to 71 % (22 HIBs out of 31 identified based on the well logging). HIB top depth error is from 5 to 66 m, except for 2x HIB – 85 m (well X3) and 113 m (well X5). The average error in estimating the depth of the HIB top is 40 m.

The results obtained in the conditions of intense man-made interference caused by stationary sources demonstrate applicability of LFS method at the producing field where it is difficult to refine the geological model using active seismic exploration methods. Practical experience in application of geological-mathematical model for LFS processing to solve the problems related to HIBs identification in the section of the Lower-Permian deposits of Kungurian stage, Irenian horizon of the Astrakhan arch confirms the method efficiency.

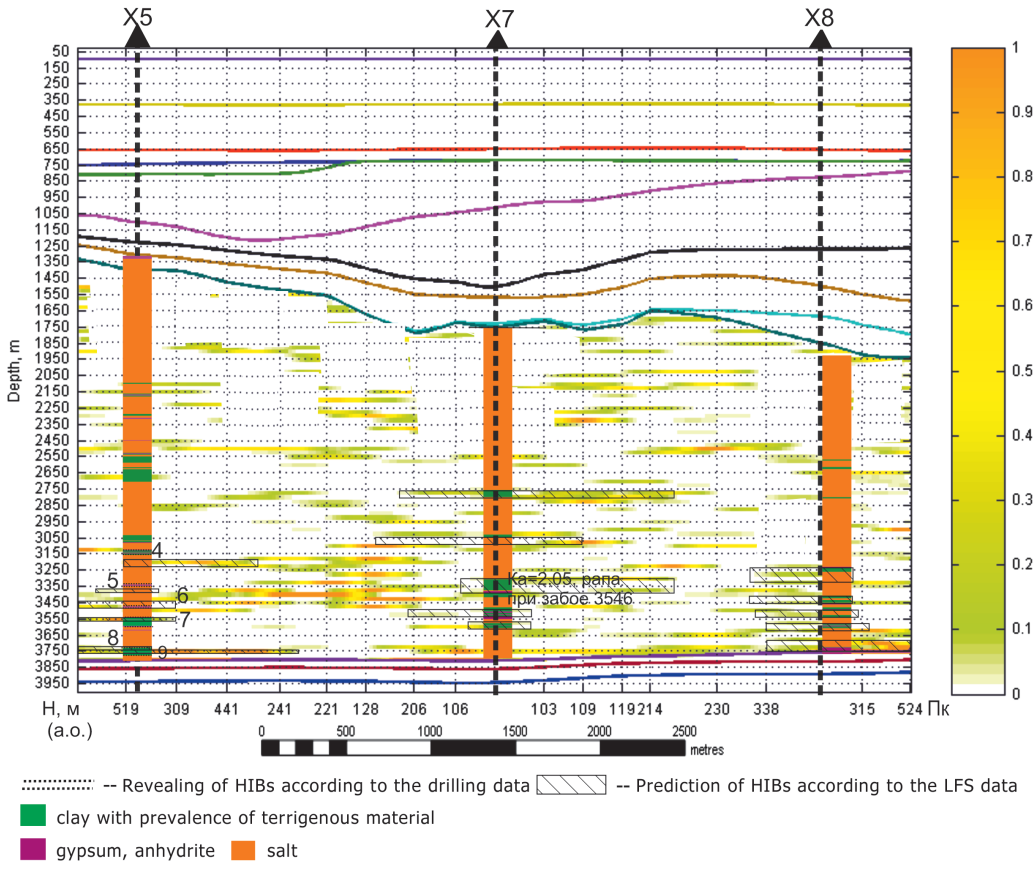

Fig. 4. HIBs identification in the sections of the LFS amplitudes

Acknowledgements

The authors thank the company Gazprom Dobycha Astrakhan for the opportunity to publish the results of the proposed approach practical application.

References

Antipov M.P. et al. (2008). The Astrakhan carbonate massif: structure and oil and gas content. Ed. Yu.A. Volozh, V.S. Parasyny. Moscow: Nauchnyy mir, 221 p. (In Russ.)

Birialtsev E. et al. (2009). Experience in Low-Frequency Spectral Analysis of Passive Seismic Data in Volga-Ural Oil-Bearing Province. *International Petroleum Technology Conference (IPTC)*, Doha, Qatar. https://doi.org/10.2523/IPTC-13678-MS

Claerbout J.F. (1968). Synthesis of a layered medium from its acoustic transmission response: *Geophysics*, 33, pp. 264–269. https://doi.org/10.1190/1.1439927

Grafov B.M. et al. (1996). Analysis of geoacoustic emission of low-frequency deposit using ANCHAR technology. *Geofizika*, 5, pp. 24–28. (In Russ.)

Draganov D., Wapenaar K., Thorbecke J. (2003). Synthesis of the reflection response from the transmission response in the presence of white noise sources: *65th Annual International Conference and Exhibition, EAGE, Extended Abstracts*, P218. https://doi.org/10.3997/2214-4609-pdb.6.P218

Haykin S. (1985). Radar array Processing for Angle-of-Arrival Estimation. Array Signal Processing, New Jersey: Prentice Hall Inc., pp. 194–292.

Kramer G. (1975). Mathematical methods in statistics. 2nd ed. Moscow. (In Russ.)

Marple S.L. (2003) Digital Spectral Analysis with Applications in C, FORTRAN, and MATLAB. Prentice-Hall.

Novikov A.A., Brazhnikov O.G., Repey A.M. et al. (2007). Prospects of searching for large oil and gas accumulations in subsalt sediments of the western part of the Pre-Caspian Basin. *Proc. Conference: Geology, resources, prospects for development of oil and gas subsoil of the Caspian basin and the Caspian region*. Moscow, pp. 30–32. (In Russ.)

Vidal et al. (2018). Passive body-wave interferometric imaging with directionally constrained migration. *Geophys. J. Int.*, 215, pp. 1022–1036. https://doi.org/10.1093/gji/ggy306

About the Authors

Evgeny V. Biryaltsev (13.02.1960–17.06.2021) – PhD (Physics and Mathematics), Director
Gradient Technology LLC
Of. 516, 50, Petersburgskaya St., Kazan, 420011, Russian Federation

Alexandra A. Vikhoreva – PhD (Physics and Mathematics)
Octopus LLC
10A, Gub. A. Guzhvin Av., Astrakhan, 414014, Russian Federation

Vasily A. Zakharchuk – PhD (Geology and Mineralogy), Head of the Geological Department
Gazprom Dobycha Astrakhan LLC
30, Lenin St., Astrakhan, 414000, Russian Federation

Alexey Yu. Komarov – Deputy Director General – Chief Geologist
Gazprom Dobycha Astrakhan LLC
30, Lenin St., Astrakhan, 414000, Russian Federation

Viktor V. Pykhalov – DSc (Geology and Mineralogy), Deputy Chief Geologist for Seismic Operations
Octopus LLC
10A, Gub. A. Guzhvin Av., Astrakhan, 414014, Russian Federation

Oleg V. Tinakin (19.11.1961–19.07. 2021) – Deputy Head of the Geological Department
Gazprom Dobycha Astrakhan LLC
30, Lenin St., Astrakhan, 414000, Russian Federation

Manuscript received 18 September 2020;
Accepted 2 April 2021; Published 30 September 2021